From diluted solid solutions to high entropy alloys: On the evolution of properties with composition of multi-components alloys

Mathilde Laurent-Brocq, Loic Perriere, Rémy Pirès, Frédéric Prima, Philippe Vermaut, Yannick Champion

Laurent-Brocq, M., L. Perrière, R. Pirès, F. Prima, P. Vermaut and Y. Champion (2017). "From diluted solid solutions to high entropy alloys: On the evolution of properties with composition of multi-components alloys." Materials Science and Engineering: A **696**: 228-235.

https://doi.org/10.1016/j.msea.2017.04.079

From diluted solid solutions to high entropy alloys: on the evolution of properties with composition of multi-components alloys

Mathilde Laurent-Brocq[1], Loïc Perrière[1], Rémy Pirès[1], Frédéric Prima[2], Philippe Vermaut[2], Yannick Champion[3]

[1] Université Paris Est, ICMPE (UMR 7182), CNRS, UPEC, F- 94320 THIAIS France

[2] PSL Research University, ChimieParisTech - CNRS, Institut de Recherche de Chimie Paris, 75005, Paris, France

[3] Univ. Grenoble Alpes, CNRS, Grenoble INP, SIMaP, F-38000 Grenoble

Corresponding author

First name: Mathilde ; Family name: Laurent-Brocq
E-mail: laurent-brocq@icmpe.cnrs.fr
Phone number : +33 (0)1 56 70 30 65
Postal adress : 2-8, rue Henri Dunant (bât D) F-94320 Thiais, France

Abstract

To study the evolution of structural and mechanical properties with composition, 10 $Cr_xMn_xFe_xCo_xNi_{100-4x}$ alloys were processed and characterized by X-ray diffraction and nanoindentation. Those alloys are all single-phase solid-solutions and their composition ranges from conventional diluted multi-component alloys (MCA) to high entropy alloys (HEA). The lattice parameter and the hardness were measured and were compared to existing models. The hardest studied alloy turns out to be the non-equimolar $Cr_{10}Mn_{10}Fe_{10}Co_{10}Ni_{60}$. More precisely, it was shown that, when the composition evolves from diluted MCA to HEA: (i) the lattice parameter increases and follows a Vegard's law up to 4x = 40 at. %; (ii) the hardness increases and follows a Mott-Nabarro-Labush law up to 4x = 40 at. % and then decreases. This breakpoint of the evolution of both lattice parameter and hardness at 40 at. % is proposed as the transition between conventional diluted multi-component solid solutions and HEA.

1. Introduction

In 2004 [1], with the idea of exploring the central region of multi-component alloy phase space, an equimolar Cr, Mn, Fe, Co and Ni alloy was produced and was unexpectedly found to be single-phased. More precisely this CrMnFeCoNi alloy is a true solid-solution, or in other words a single crystalline structure on which several elements are randomly distributed [2]. This was an innovative suggestion. Indeed, for a long time, metallic alloys were restricted to one or two principal elements, in order to avoid complex multi-phases microstructures, as the ones observed in binary or ternary phase diagrams when the concentration of a minor element is increased. Also in 2004, Yeh *et al.* [3] suggested that concentrated multi-component solid solutions should be stabilized by configurational entropy, which is maximized for an equimolar composition and which increases with the number of element. The name "high entropy alloys" (HEA) was proposed and defined as alloys composed of five or more elements in equimolar ratios or, in an extended definition with concentration between 5 and 35 at. % [3]. Gradually, the name HEA was more and more used for those single-phase alloys, although pioneering works [1, 3] were not restricted to a single-phase state. In the following, the name HEA will refer to very concentrated multi-component single-phase solid-solution while terms as multi-principal element alloy or complex concentrated alloys will be used for multi-phase microstructures [4].

In the initial HEA concept [3], a thermodynamic description of HEA, based on the condition of maximizing the configurational entropy, was put forward. However, since then, it has been clearly established that maximizing the configurational entropy is neither a sufficient nor a necessary condition to form a multi-component solid-solution [5]. Indeed, among the numerous multi-component equimolar alloys which have been studied, some form solid-solution, like VNbMoTaW [6] and TiZrNbHfTa [7], but many are multi-phased, like in the alloy AlCrFeCoNiCu [8]. Lately, the composition range of stability of the fcc solid-solution was entirely mapped for the Cr-Mn-Fe-Co-Ni system [9]. It was shown that thermodynamic laws which are used to describe binary and ternary alloys can also be applied to HEA. In other words, there is no thermodynamic specificity of HEA compared to conventional alloys.

Following the discovery of HEA, advantageous combinations of strength and ductility have been measured on several quinary equimolar HEA [10-15]. They have raised a great interest on HEA. At first, those unforeseen mechanical properties were proposed to be due to a severe lattice distortion [16], which would be involved by the specific structural organization of HEA (i.e. : a high number of concentrated elements, which can all be considered as solute). Lately, the fact that the lattice distortion is more severe in HEA than in conventional alloys has been put into doubts [17], especially for the equimolar CrMnFeCoNi HEA [18]. To determine whether HEA have structural and, as a consequence, mechanical specificities compared to conventional alloys, a study of a large number of non-equimolar solid-solutions on a wide range of chemical compositions is needed. Indeed, lately some non equimolar HEA have been studied [19-22] but with only restricted composition variations, such as adding from 0 to 8 at. % of Al in a CrMnFeCoNi alloy [21] or making varying the Mn content of around 15 at. % in a $Fe_{64-x}Mn_xNi_{28}Co_5Cr_2$ [22].

In this context, it is proposed to investigate the evolution of structural and mechanical properties of multi-components alloys when the composition evolves from diluted solid solutions towards very concentrated solid solution (i.e.: HEA). The objective of this study is to determine whether properties continuously evolve, which would mean that HEA are qualitatively similar to diluted solid solutions; or whether there is a break point in properties evolution which would reflect a specificity of HEA. 10

$Cr_xMn_xFe_xCo_xNi_{100-4x}$ alloys, with x varying between 2 and 20, were chosen to be studied. All those alloys were already proven to form single solid-solution [23]. This wide range of composition allows to compare conventional diluted MCA (i.e. low value of x) with HEA (when Cr, Fe, Mn and Co content are similar to Ni content, i.e. values of x close to 20) and to study the transition between both. It is underlined that, for now, diluted solid-solutions and HEA cannot be quantitatively defined.

The 10 $Cr_xMn_xFe_xCo_xNi_{100-4x}$ alloys were processed and characterized by X-ray diffraction and nanoindentation in order to measure their lattice parameter and hardness. The experimental results were compared to existing models, which were developed either for conventional diluted solid solutions or for HEA.

2. Experimental

10 $Cr_xMn_xFe_xCo_xNi_{100-4x}$ multi-component alloys were processed, where x takes the values of 2, 3, 4, 7.5, 10, 12.5, 15, 17.5, 18.75 and 20. Samples are named according to their Cr, Mn, Fe and Co content which is equal to 4x (in at. %). For example $Cr_{10}Fe_{10}Mn_{10}Co_{10}Ni_{60}$ and $Cr_{20}Fe_{20}Mn_{20}Co_{20}Ni_{20}$ alloys are respectively named MCA-40 and MCA-80. For low values of x, 4x represents the solute content. For larger values of 4x, the distinction between solute and solvent becomes irrelevant. All alloys were prepared with the same procedure, which has been previously developed for the equimolar alloy CrMnFeCoNi [2] and which was presented in details in [5]. The main steps of the processing are recalled. First, raw Co, Cr, Fe, Mn and Ni metals were melted by high frequency electromagnetic induction melting in a water-cooled copper crucible under He atmosphere. Then suction casting was performed to shape the ingots into a rod with a diameter of 3 mm. Finally some slices of the rod, wrapped in a tantalum sheet, were annealed at 1100°C for 6 h under an He atmosphere. At the end of annealing, still maintained in the He atmosphere, the samples were quickly cooled down. To ensure reproducibility, for three compositions (4x = 40, 70 and 80), the entire processing procedure was performed twice. For 2 samples having the same composition, the difference between their lattice parameter or their hardness is smaller than the experimental uncertainty. It guarantees that the processing procedure and the characterization analysis are reproducible.

A Merlin Zeiss microscope, which is equipped with a field emission gun, was used for Scanning Electron Microscopy (SEM). The grains of samples were observed by using the backscattered electron detector (BSE) at a low magnification (× 30) and with a 15 kV beam. X-ray diffraction (XRD) was performed in a PANalytical X'Pert Pro diffractometer using the Co–K_α radiation at a wavelength of 0.178897 nm.

Nanoindentation was performed with a TI 950 Hysitron indenter, which was equipped with a Berkovich tip. Before testing, samples were mechanically polished with abrasive papers of silicon carbides and afterwards with diamond pastes containing particles with sizes down to 0.25 µm. It is mentioned that such a polishing procedure does not completely remove the hardening surface layer which is created by the first polishing step. Still, since all samples underwent the same polishing procedure, it is considered that, in a comparative approach, the effect of this hardening layer can be neglected. The agreement of our measurements with another study of HEA by nanoindentation [24] confirms this assumption (see 3.1). Scanning Probe Microscopy, which consists in scanning the sample surface with the nanoindenter tip, was used to register 10 × 10 µm² images of the surface topography. Values between 1.2 and 3.3 nm and between 0.3 and 1.5° were determined for roughness and tilt respectively. Thus indents with a maximum depth of 300 nm as performed here are not influenced by the surface quality of the sample [25]. Due to the indentation size effect (ISE), the measured hardness on a given

material decreases with indent depth [26]. To obtain a similar ISE and thus comparable hardness values, indents were performed with a constant maximum depth of 300 nm. This corresponds to maximum applied load between 6 and 9.5 mN, depending on the sample. For each indentation, the loading and unloading rates were 1 $mN.s^{-1}$ and the maximum load was maintained during 2 s. Hardness and reduced elastic modulus were determined from the loading-unloading curves by using the Oliver and Phar model [27].

First MCA-40, MCA-70 and MCA-80 were deeply investigated. A minimum of 10 rectangular patterns of 20 indents, whose separation distance is 20 µm, were randomly distributed all over the sample surface. Each pattern covered an area of 80 x 60 μm^2. No significant difference between the average hardness and Young's modulus of each group were found. It guarantees that samples are homogeneous and that the average values over one group of indents can be considered as representative of the whole sample. Moreover, in this procedure, different grains, and thus different crystallographic orientations, have been tested. Consequently, the influence of crystallographic orientation on measurement, if any for those materials, is lower than the experimental uncertainty and can be neglected. For other samples, one group of 20 indents, was performed. The given hardness and Young's modulus values and uncertainties are respectively the average and the standard deviation on those 20 measurements. It is mentioned that the uncertainty on the nanoindentation absolute values of hardness and Young's modulus is respectively 10% and 5%. However, in a comparative approach, the uncertainty on hardness is lower, as are the given standard deviations.

3. Results and discussion

3.1. Lattice parameter

The MCA-4x alloys were analyzed by XRD and they all exhibit similar patterns, i.e. four peaks corresponding to the fcc phase. Patterns of MCA-8 and MCA-80 are plotted on Fig. 1a. There is a shift of the peak position, depending on the alloy composition, which reflects a variation of the lattice parameter. The lattice parameters of the fcc phase, which were determined from the XRD patterns, are plotted according to 4x on Fig. 1b. The values of MCA-8, MCA-40 and MCA-80 are given in Table 1. Qualitatively, when 4x increases, it can be seen that: (i) the lattice parameter increases, (ii) the derivative changes for 4x around 40 at. %.

Then, the Vegard's law was applied to the MCA-4x alloys. It can be written as:

$$a_{Vegard}(4x) = a_{Ni} \cdot \frac{1-4x}{100} + \frac{x}{100} \cdot (a_{Cr} + a_{Mn} + a_{Fe} + a_{Co}) \qquad (1)$$

where a is the lattice parameter and x is the content of Cr, Mn, Fe or Co in at. %. For all elements, in order to consider comparable interatomic distances, fcc phases were considered. It corresponds to the structure at room temperature for Ni, whose lattice parameter is 3.5238 Å [28], and to high temperature structures for Mn, Fe and Co, whose lattice parameters are respectively 3.8624 Å, 3.6468 Å and 3.5440 Å [28]. For Cr, since the fcc phase is not stable at any temperature [28], the lattice parameter is calculated from fcc Ni-Cr alloys [28]. As proposed in [29], the Vegard's law is applied, i.e. $a_{Ni-\delta Cr} = (1-\delta) \cdot a_{Ni} + \delta \cdot a_{Cr}$, where δ is the atomic fraction of Cr in the alloy Ni-δCr. A lattice parameter of 3.6526 Å for a pure fcc Cr is deduced. Thus, for MCA-4x alloys, the following Vegard's law can be written: $a_{Vegard} = 1.527 \cdot 10^{-3} \cdot 4x + 3.5238$, where a is in Å and x in at. %. It was plotted

on Fig. 1b. It is underlined that this law is not fitted on experimental data. It appears that the Vegard's law is in very good agreement with the experimental data for alloys such as $8 \leq 4x \leq 40$. When 4x increases further, the experimental lattice parameters become smaller than the Vegard's prediction. In other words, for $4x > 40$ at.%, the lattice parameter becomes denser than the Vegard's prediction. It means that there is no modification of the electronic structure and of the inter-atomic distances until around 40 at. % of Cr, Mn, Fe and Co [30]. For this range of composition, the lattice parameter increases only because of a modification of the proportion of each type of inter-atomic distances. As a comparison, for Ni-X binary alloys, the evolution of the lattice parameter is linear up to 100, 58, 40 and 25 at. % for respectively Co, Fe, Cr and Mn [30]. Thus the amount of solute that can be added without modification of inter-atomic distances for the fcc Ni phase is lower in a multi-component alloy than in binary alloys (except for Mn).

It could be argued that the Vegard's law, which is only based on pure elements lattice parameters, is not relevant to take into account the wide variety of inter-atomic distances in a multi-component alloy. Thus another approach, which was specifically developed for HEA by Toda-Carabello *et al.* [31], was also applied to MCA-4x alloys (Appendix 1). In this model, the lattice parameter is computed as the average of inter-atomic distances weighed by the composition. The inter-atomic distances are deduced from data on binary alloys and are considered constant. For CrMnFeCoNi quinary MCA, there are 15 different inter-atomic spacings. As for the Vegard's law, the Toda-Carabello model consistently describes the diluted MCA but not the HEA. It leads to the same conclusion: when the Cr, Mn, Fe and Co contents is large enough, the inter-atomic distances are very likely modified.

It was shown that, when $4x = 40$ at. %, there is a breakpoint in the lattice parameter evolution with composition: (i) the derivative according to the composition decreases, (ii) the lattice parameter goes away from the Vegard's law. This could be indicative of a transition between diluted MCA and HEA. It is mentioned that the equimolar CrMnFeCoNi alloy is paramagnetic at room temperature and above [32]. Thus a transition from paramagnetic to magnetic state when increasing x is very unlikely. It is proposed that this evolution of the lattice parameter could be due to short range ordering (SRO). SRO has never been experimentally and directly observed either by atom probe tomography [2, 19, 20, 22], or by X-ray and neutron scattering [33], or by high resolution EDS [34]. However, detecting SRO in such a compositionally complex system, especially if it is partial, is certainly an experimental challenge as underlined in [17]. Very recently, a transition in specific heat measurements according to temperature on equimolar HEA alloys from the Cr-Mn-Fe-Co-Ni system was measured, which could be attributed to a short-range order/disorder transitions [32]. Besides, Tamm *et al.* [35] clearly identified SRO in equimolar NiCrCo and NiCrCoFe alloys by Monte Carlo method combined with ab-initio calculations and they also calculated that this SRO would not be detectable by EXAFS. Additional studies are needed to generalize and confirm the occurrence of SRO for HEA.

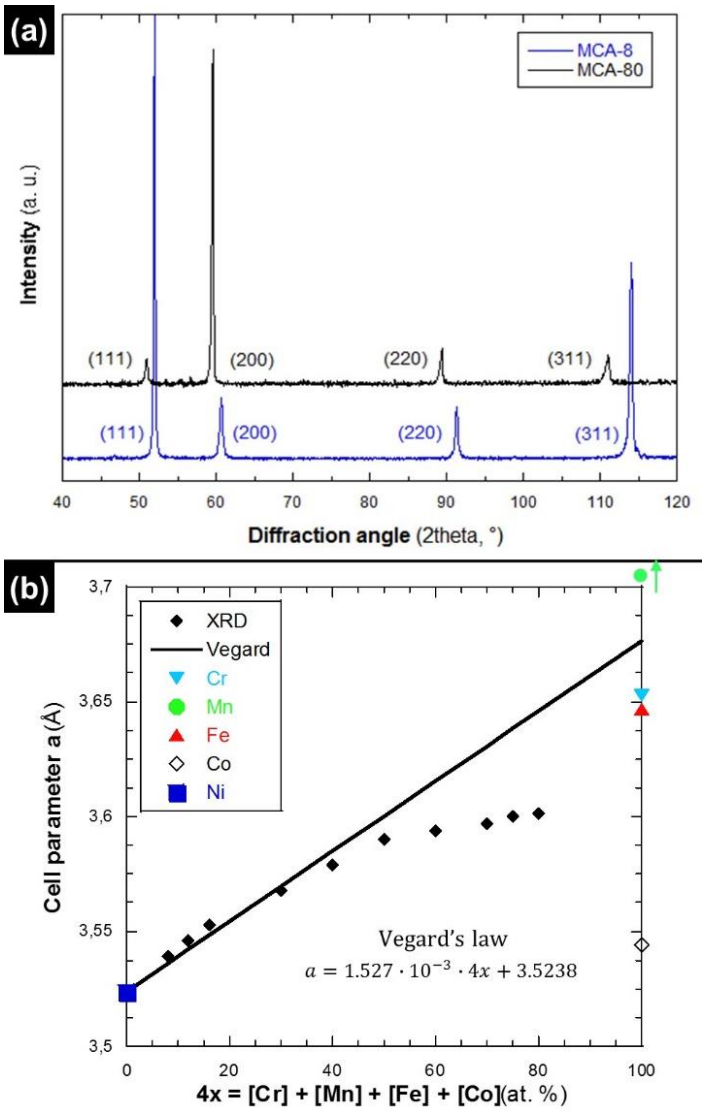

Fig. 1 (Color online): X-ray diffraction. (a) XRD patterns of MCA-8 and MCA-80. The crystallographic planes of the face-centered cubic (fcc) phase are indicated near to the corresponding peaks. Those patterns are representative of all MCA-4x samples. (b) Lattice parameters of the fcc phase for the 10 MCA-4x processed alloys. Error bars are smaller than the symbols. A Vegard's law is plotted and its equation is given. The pure metal fcc lattice parameters are also indicated.

Table 1 : Lattice parameter, hardness and Young's modulus of MCA-8, MCA-40 and MCA-80 as measured by respectively X-ray diffraction and nanoindentation. The nominal composition of samples is also indicated.

Sample name	Composition	Lattice parameter (Å)	Hardness (GPa)	Young's modulus (GPa)
MCA-8	$Cr_2Fe_2Mn_2Co_2Ni_{92}$	3.539 ± 0.001	2.41 ± 0.08	194 ± 10
MCA-40	$Cr_{10}Fe_{10}Mn_{10}Co_{10}Ni_{60}$	3.579 ± 0.002	3.72 ± 0.16	201 ± 10
MCA-80	$Cr_{20}Fe_{20}Mn_{20}Co_{20}Ni_{20}$	3.601 ± 0.003	3.09 ± 0.10	189 ± 9

3.2.Hardness

Afterwards, the MCA-4x alloys were studied by nanoindentation. First, it was checked that the influence of crystallographic orientation on measurement, if any for those materials, is lower than the experimental uncertainty and can be neglected (see 2). Second, since all MCA-4x were homogeneized in the same way (i.e. high temperature and long duration), the density of pre-existing dislocations is considered to be low and similar in all samples. In a comparative approach, the strengthening effect of pre-existing dislocations is thus neglected. Third, it was checked that grain boundary strengthening had no influence on nanoindentation hardness measurements. Indeed, the grain size of all MCA-4x samples is larger than 100 µm (Appendix 2), which is several order of magnitude larger than the indent depth (i.e. 300 nm, see 2). Consequently, as already proposed in [36], nanoindentation measurements will allow solid solution hardening to be studied.

The loading-unloading curves of MCA-8, MCA-40 and MCA-80 are plotted on Fig. 2a. They exhibit no peculiarities and are representative of all MCA-4x alloys. Hardness and Young's modulus were determined from those curves. The hardness is plotted according to 4x on Fig. 2b. The values of MCA-8, MCA-40 and MCA-80 are given in Table 1. MCA-80 (i.e. the CrMnFeCoNi equimolar alloy) has an hardness of 3.09 ± 0.10 GPa. This is in very good agreement with the hardness measured by nanoindentation at a similar depth on an homogeneized equimolar CrMnFeCoNi in [24]. As expected, MCA-80 is harder than conventional diluted solid-solution, like MCA-8 whose hardness has a value of 2.41 ± 0.08 GPa. However, interestingly, MCA-80 is not the harder MCA-4x alloy. Indeed, when 4x increases, the hardness increases up to 3.72 ± 0.16 GPa for 4x = 40 at. % and then it decreases until 4x = 80. MCA-40 hardness is around 20 % and 50 % larger than MCA-80 and MCA-8 respectively. It is recalled that the configurational entropy is maximized for MCA-80. In other words, the maximum of configurational entropy does not correspond to the maximum of hardness. It has already be proven that equimolar solid solutions with a lower number of elements, and thus with a lower configurational entropy, could have a higher yield strength than their quinary counterpart [37, 38]. This study also proves that non equimolar quinary solid-solutions can exhibit an improved hardness compared to the well-studied CrMnFeCoNi alloy.

Existing analytical models of solid solution strengthening are considered. In fcc alloys, the flow stress τ_c can be described by: $\tau_c = \tau_P + \alpha \cdot c^{\beta}$ (2) where τ_P is the Peierls stress of the pure metal, c is the solute concentration, α and β are material constants which depend respectively on the strength of the dislocation-solute interaction and on the strengthening statistics. In the Mott-Nabarro-Labush (MNL) model [39], which was developed for concentrated solid-solution, β is equal to 2/3. Following Tabor's work [40], equation (4) is transposed to hardness: $H = H_0 + A \cdot c^r$ (3) where H_0 is the hardness of the pure metal and A and r are material constants. As in MNL model, r is set to 2/3. The constant A cannot be determined *a priori* as proposed in MNL models for binary alloys because too many data would be needed for the multi-component alloys which are studied here. Instead, A and H_0 were determined by fitting the data for alloys such as 8 ≤ 4x ≤ 30. It gives: $H = 1{,}91 + 0{,}76 \cdot (4x)^{2/3}$, with a high regression coefficient (R^2=0.92). The hardness of MCA-4x alloys is consistently described by the MNL model for 8 ≤ 4x ≤ 40, i. e. the increasing domain.

To calculate the Young's modulus from the reduced elastic modulus measured by nanoindentation, the Poisson's ratio of the alloy is needed [41]. Poisson's ratios of 0.304 and 0.265, which were measured on pure Ni and on an equimolar CrMnFeCoNi respectively [42], were used for MCA-8 and MCA-80. For MCA-40, not knowing the Poisson's ratio, a value of 0.284, which is the average of the

two above-mentioned values, was used. The Young's modulus of MCA-8, MCA-40 and MCA-80 are given in Table 1. The Young's modulus of MCA-80 is in very good agreement with the value found by resonant ultrasound spectroscopy on the same alloy [42]. However, given an uncertainty of 5% for measurement of Young's modulus by nanoindentation and not knowing the Poisson's ratio, no tendency between Young's modulus and MCA-4x composition can be drawn for now.

When 4x = 40 at. %, there is a breakpoint in the hardness evolution with composition: (i) the hardness is maximum, (ii) the hardness goes away from the MNL law. Noteworthy, the breakpoint of lattice parameter takes place at the same composition. Thus 4x = 40 at. % is proposed as the transition between conventional (i.e. diluted) multi-component solid solutions and high entropy alloys.

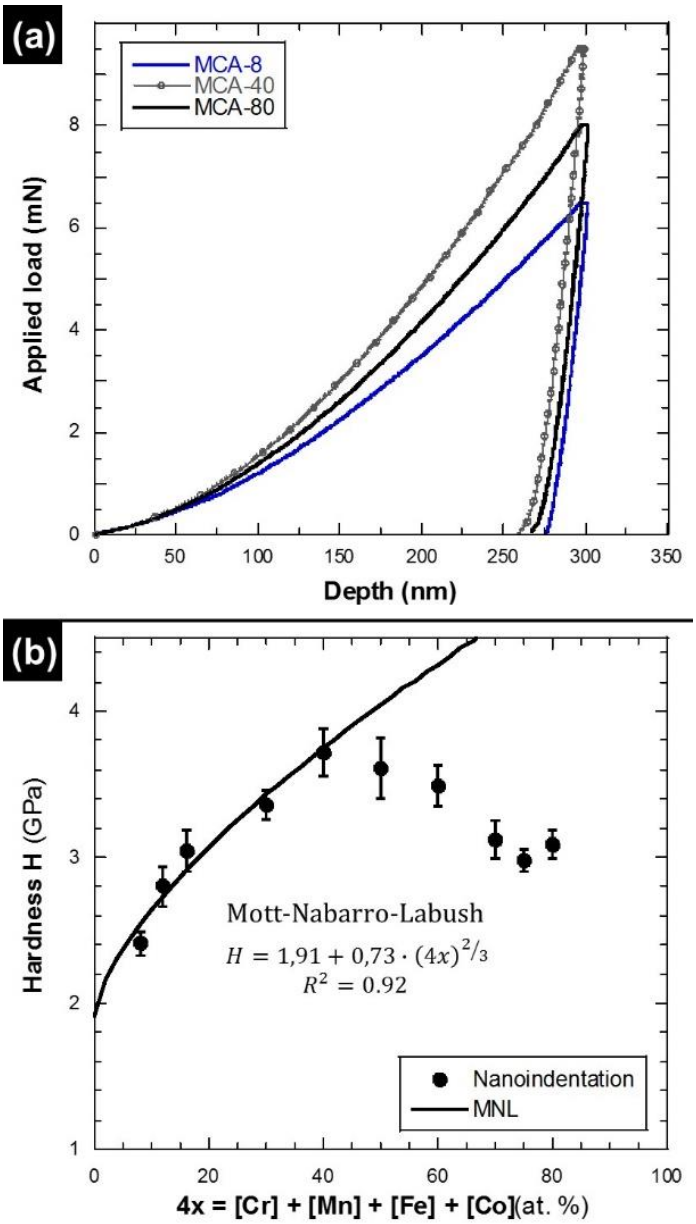

Fig. 2 : Nanoindentation measurements. (a) Loading-unloading curves of MCA-8, MCA-40 and MCA-80 with a maximum depth of 300 nm. Those curves are representative of all MCA-4x processed alloys. (b) Hardness of the 10 processed MCA-4x alloys. Error bars are the standard deviation of measurements. A Mott-Nabarro-Labush (MNL) law, which was fitted on alloys for which 4x ≤ 30, is plotted. The equation and regression coefficient are given.

3.3. Modeling of solid solution strengthening

To explain the evolution of lattice parameter and hardness which was previously exposed, a theory of strengthening which was lately developed for fcc high entropy alloys [29], is applied to $Cr_xMn_xFe_xCo_xNi_{100-4x}$ alloys. The key principle of this model is to consider each element of the alloy as a solute embedded in the effective matrix, which has the average properties of the alloy. Based on this principle, a model of solute strengthening in dilute alloys was extended to HEA. We use the reduced model, which considers only the elastic contribution to the solute/dislocation interaction energy and which has the advantage to be fully analytic. This reduced model has already provided prediction in good agreement with experimental data for equimolar alloys of the Cr-Mn-Fe-Co-Ni system [29]. According to equation (15) of [29], the zero-temperature flow stress τ_{Y0} is defined as:

$$\tau_{Y0} = B \cdot \left(\frac{\sum_n c_n \cdot (\Delta V_n)^2}{b^2} \right)^{2/3} \quad (4)$$

Where:

- $B = 0.051\alpha^{-\frac{1}{3}} \cdot \mu \cdot \left(\frac{1+\nu}{1-\nu}\right)^{\frac{4}{3}} \cdot f_1(w_c)$ (5) with α a dislocation line tension parameter, μ and ν the isotropic elastic constants and $f_1(w_c)$ the dislocation core coefficient
- c_n is the atomic fraction of element n
- ΔV_n is the volume misfit of element n and is defined as $\Delta V_n = \bar{V} - V_n = (\sum_n c_n \cdot V_n) - V_n$ (6), with $\bar{V}$ the average atomic volume of the alloy and V_n the individual atomic volume of element n
- b is the Burger's vector

First the average atomic volume $\bar{V}$ of the MCA-4x is calculated, using as individual atomic volume 12.27, 12.6, 12,09, 11.12 and 10.94 $Å^3$ respectively for Cr, Mn, Fe, Co and Ni, as proposed in [29]. It is mentioned that, for Ni, this volume corresponds to the fcc room temperature, for Cr, Fe and Co, those volumes were calculated from binary Ni-X fcc solid solutions (where X is Cr, Fe or Co), and for Mn, the volume is deduced by combining the average atomic volume of equimolar HEA alloys and the individual atomic volume of the other elements. Moreover, the lattice parameters which were measured by XRD (see 3.1) are converted into average atomic volume (i.e.: $\bar{V} = \frac{a^3}{4}$). The calculated and measured average atomic volumes of MCA-4x alloys are plotted on Fig. 3a. On the whole, there is a reasonable agreement between experiment and calculation. However, the change of the derivative of the average atomic volume for 40 at. % which was measured by XRD is not reproduced by calculation. Indeed, the evolution of the calculated average atomic volume is linear for the whole range of composition. This is due to the fact that, in this approach, the individual atomic volumes are considered constant, whatever the alloy composition. On the contrary, based on XRD lattice parameter measurements, it was proposed that the inter-atomic distances evolves with the composition, due to short range ordering (see 3.1).

Second, for each element and for each composition, the volume misfit ΔV_n is calculated according to equation ΔV_n is the volume misfit of element n and is defined as $\Delta V_n = \bar{V} - V_n = (\sum_n c_n \cdot V_n) - V_n$ (6). As an example, ΔV_{Fe} is indicated with red arrows on Fig. 3a. ΔV_{Fe} decreases when 4x increases. The trend is the same for ΔV_{Cr} and ΔV_{Mn}. On the contrary, ΔV_{Ni} (blue arrows on Fig. 3a) increases when 4x

increases, as for ΔV_{Co}. Third, the volume misfit is multiplied by the concentration of each element (Fig. 3b). Since ΔV_{Fe} decreases and c_{Fe} increases when 4x increases, $\Delta V_{Fe}^2 \cdot c_{Fe}$ exhibits a maximum, as for Cr and Mn. For Ni, ΔV_{Ni} increases and c_{Ni} decreases when 4x increases, thus $\Delta V_{Ni}^2 \cdot c_{Ni}$ also exhibits a maximum. Finally $\Delta V_n^2 \cdot c_n$ of all elements are added and divided by the Burger's vector (equation (4)). In a first approximation, B is considered as constant for all MCA-4x alloys. In [29], α and $f_1(w_c)$ are also considered as constants. Here, since the elastic constants of MCA-4x alloys are only partially known (see 3.2), they are considered as constant. To be able to compare with the measured hardness, the flow stress is normalized by the flow stress of MCA-80. The normalized hardness and flow stress are plotted on Fig. 3c. It can be seen that there is a good qualitative agreement between experimental data and the model. Especially, a maximum of flow stress for a non-equimolar composition is predicted. However, there are some quantitative disagreement between the maximum of the measured hardness and the one of the calculated flow stress: (i) they do not correspond to the same composition of the alloy and (ii) the value is underestimated by the calculation. The main reason of this quantitative disagreement is very likely due to the volume misfits, which were chosen as input data for the theory and which are only in reasonable agreement with experimental lattice parameter. Thus an improvement in the description of the atomic structure of HEA is needed. The fact that the evolution of the elastic constants with the composition is not known and the fact that we compare hardness and flow stress, which do not represent exactly the same mechanical properties, could also have an influence, probably in a lesser extent.

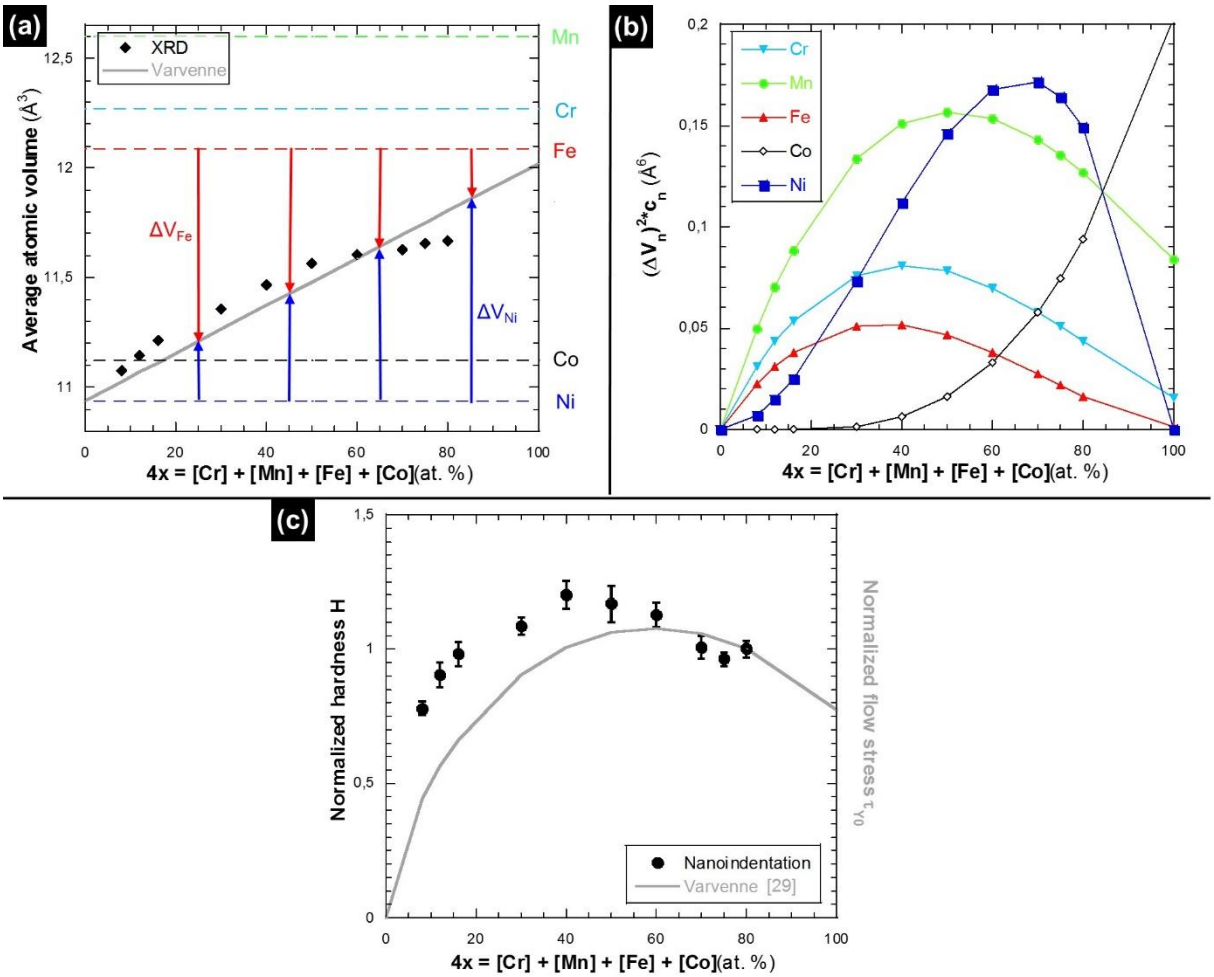

Fig. 3 : Application of the theory of strengthening of Varvenne et al. [29] to MCA-4x alloys. (a) Average atomic volumes as measured by XRD (full diamond) and as predicted by the theory of Varvenne et al. [29] (grey line). The atomic volumes of the pure metals which were used in the model are indicated as dashed lines. The volume misfit ΔV is represented by arrows for Fe and Ni as an example. (b) Evolution with the composition of $(\Delta V_n)^2 \cdot c_n$ *, with* ΔV_n *and* c_n *respectively the volume misfit and the atomic fraction of element n. (c) Normalized hardness H as measured by nanoindentation and normalized flow stress* τ_{Y0} *as predicted by the theory. H and* τ_{Y0} *are normalized by the value of MCA-80.*

4. Conclusion

10 $Cr_xMn_xFe_xCo_xNi_{100-4x}$ alloys, which are all single-phase solid-solutions and whose composition ranges from conventional diluted multi-component alloys (MCA) to high entropy alloys (HEA), were processed by induction melting, casting and homogeneization annealing and then characterized by X-ray diffraction and nanoindentation. Thus lattice parameter as well as the hardness were measured for the 10 alloys. A theory of solid-solution strengthening, which was developed in [29], was applied to those 10 alloys and the calculation data were compared to the experimental results.

The main results are the following:

- The hardest alloy out of the 10 which were studied is $Cr_{10}Mn_{10}Fe_{10}Co_{10}Ni_{60}$. In other words, the hardest alloy is non equimolar.
- When 4x (i.e. the content of Cr, Mn, Fe and Co) increases: (i) the lattice parameter increases and follows a Vegard's law up to 4x = 40 at. % and then it goes away from the Vegard's law; (ii)

the hardness increases and follows a Mott-Nabarro-Labush law up to 4x = 40 at. % and then decreases.
- This breakpoint of the evolution of both lattice parameter and hardness at 40 at. % is proposed as the transition between conventional diluted multi-component solid solutions and HEA.
- The theory of solid solution strengthening developed in [29] is in good qualitative agreement with the hardness measurements, with however some quantitative discrepancies. An improvement of the local atomic structure description and especially of the volume misfit of HEA is needed to provide better input data for the model.

In a future work, the most promising alloy $Cr_{10}Mn_{10}Fe_{10}Co_{10}Ni_{60}$ will be studied by tensile tests and an approach similar to the one proposed here for Ni will be developed to study the effect of Cr, Mn, Fe and Co on the mechanical behavior of CrMnFeCoNi alloys. Thanks to those additional experimental data, the theory of solid solution strengthening could be further improved.

Appendix 1

The model which was developed by Toda-Carabello *et al.* [31] to calculate HEA lattice parameter was applied to the MCA-4x alloys. In this model, the lattice parameter is computed as the average of inter-atomic spacings weighed by the composition. The inter-atomic spacings are deduced from data on binary alloys and are considered constant. The main formula defined in [31] are recalled. First, the interatomic spacings are defined as:

$$s_{ij} = \frac{s^{ave} - s_{ii} \cdot X_i^2 - s_{jj} X_j^2}{2 \cdot X_i \cdot X_j} \qquad (7)$$

Where :

- $s_{i,j}$ is the interatomic spacing between species i and j,
- s^{ave} is the average interatomic spacing of the binary alloy. $s_{ave} = f \cdot a$ (8) where a is the lattice parameter and $f = 1/\sqrt{2}$ or $f = \sqrt{3}/2$ for respectively fcc and bcc alloys,
- X_i and X_j are the atomic fraction of species respectively i and j.

For each of the 10 binary systems, lattice parameters of various binary compositions were collected in [43] and then were used to calculate $s_{i,j}$. Then the obtained values were averaged. The number of $s_{i,j}$ for each binary alloys depends on data availability and on the size of the miscibility area. For example, for Co-Mn, 9 values of $s_{i,j}$, which correspond to alloys whose composition varies from 20 to 54 at. % of Mn, were averaged, while for Co-Cr, 3 values of $s_{i,j}$, which correspond to alloys whose composition varies from 22 to 30 at. % of Co, were averaged. The relative standard deviations on the averaged $s_{i,j}$ vary from 0.1% up to 4%. It is underlined that the determination of the $s_{i,j}$ appears ambiguous (i.e. it depends on the chosen data and it can lead to large standard deviations). All the $s_{i,j}$ data are summarized in Table 2.

Table 2 : Interatomic spacings of binary alloys which were calculated with formula (7). The values of bcc alloys are written in italic.

S(i,j)	**Cr**	**Mn**	**Fe**	**Co**	**Ni**
Cr	2,49760	*2,32401*	*2,35073*	*2,29620*	2,52666
Mn	*2,32401*	2,73110	2,47338	2,50360	2,65352
Fe	*2,35073*	2,47338	2,57870	2,54239	2,53335
Co	*2,29620*	2,50360	2,54239	2,50600	2,49897
Ni	2,52666	2,65352	2,53335	2,49897	2,49170

Then the average interatomic spacing of each alloy MCA-4x is calculated:

$$s^{ave} = (X^A)^T * S_{i,j} * X^A$$

Where X^A is the vector of the concentration (in atomic fraction) of alloy A. $(X^A)^T=(X_{Cr}\ X_{Mn}\ X_{Fe}\ X_{Co}\ X_{Ni})$

Then s^{ave} is converted in a lattice parameter with formula (6). The calculated values of lattice parameters are plotted together with the experimental values on Fig. 4. It can be seen that, as for the Vegard's law, the Toda-Carabello model consistently describes the diluted MCA but not the HEA, either quantitatively or qualitatively.

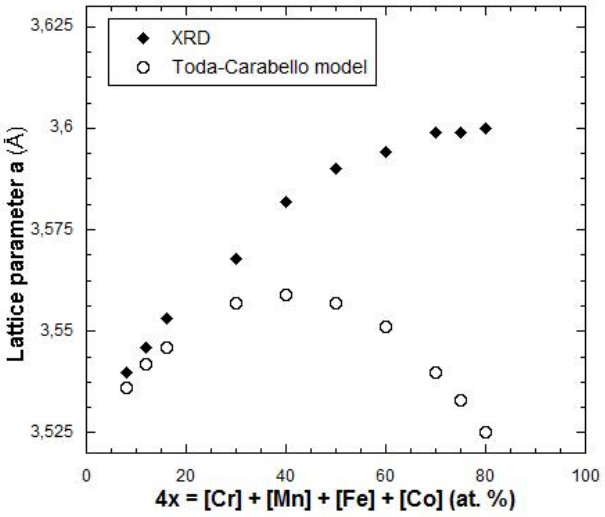

Fig. 4 : Lattice parameters of MCA-4x alloys as measured by XRD and as calculated based on the Toda-Carabello model [31]

Appendix 2

The images for MCA-8 and MCA-80 are depicted on Fig. 5. Both exhibit large, elongated and irregular grains. This comes as no surprise since no thermo-mechanical treatments, such as rolling or recrystallization annealing, were performed. For MCA-8, width and length vary respectively between 90 and 450 µm and between 220 and 620 µm. For MCA-80, the width varies between around 90 and 180 µm while the length varies between around 250 and 1000 µm. Other MCA-4x samples are in between those 2 cases, with no direct correlation between the chemical composition and the grain size. Thus, the 10 single-phase samples exhibit different grain size, but with a characteristic dimension larger than 100 µm for all of them.

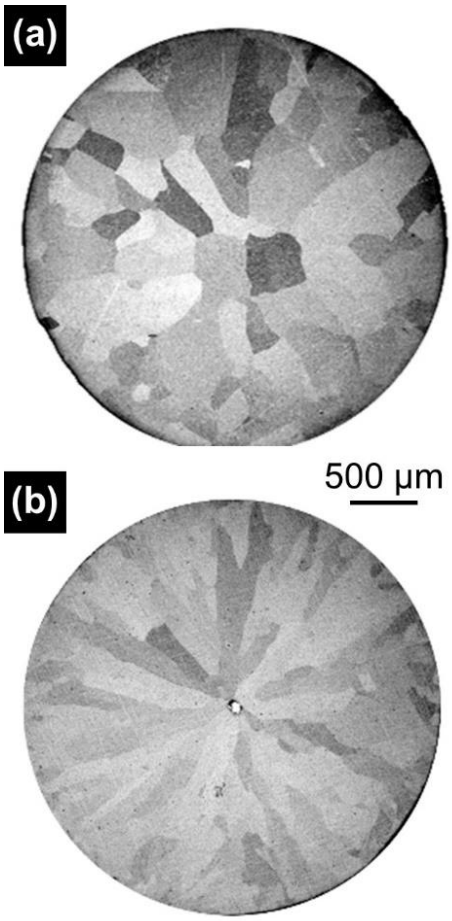

Fig. 5 : Scanning Electron Microscope (SEM) images with a Back-Scattered Electron (BSE) dectector of transversal cross-sections of (a) MCA-8 and (b) MCA-80. Grains are anisotropic, with irregular shape and characteristic dimension larger than 100 µm. Those images are representative of all MCA-4x samples.

5. References

[1] Cantor, B., I.T.H. Chang, P. Knight, and A.J.B. Vincent, *Microstructural development in equiatomic multicomponent alloys.* Materials Science and Engineering: A, **2004**. 375–377: p. 213-218.

[2] Laurent-Brocq, M., A. Akhatova, L. Perrière, S. Chebini, X. Sauvage, E. Leroy, and Y. Champion, *Insights into the phase diagram of the CrMnFeCoNi high entropy alloy.* Acta Materialia, **2015**. 88 (0): p. 355-365.

[3] Yeh, J.W., S.K. Chen, S.J. Lin, J.Y. Gan, T.S. Chin, T.T. Shun, C.H. Tsau, and S.Y. Chang, *Nanostructured high-entropy alloys with multiple principal elements: Novel alloy design concepts and outcomes.* Advanced Engineering Materials, **2004**. 6 (5): p. 299-303.

[4] Miracle, D.B. and O.N. Senkov, *A critical review of high entropy alloys and related concepts.* Acta Materialia, **2017**. 122: p. 448-511.

[5] Laurent-Brocq, M., L. Perrière, R. Pirès, and Y. Champion, *From high entropy alloys to diluted multi-component alloys: Range of existence of a solid-solution.* Materials & Design, **2016**. 103: p. 84-89.

[6] Senkov, O.N., G.B. Wilks, D.B. Miracle, C.P. Chuang, and P.K. Liaw, *Refractory high-entropy alloys.* Intermetallics, **2010**. 18 (9): p. 1758-1765.

[7] Couzinié, J.P., G. Dirras, L. Perrière, T. Chauveau, E. Leroy, Y. Champion, and I. Guillot, *Microstructure of a near-equimolar refractory high-entropy alloy.* Materials Letters, **2014**. 126 (0): p. 285-287.

[8] Singh, S., N. Wanderka, B.S. Murty, U. Glatzel, and J. Banhart, *Decomposition in multi-component AlCoCrCuFeNi high-entropy alloy.* Acta Materialia, **2011**. 59 (1): p. 182-190.

[9] Bracq, G., M. Laurent-Brocq, L. Perrière, R. Pires, Y. Cotrebil, V. Lalanne, I. Guillot, and J.-M. Joubert, *Phase stability of CoCrFeMnNi multi-components alloys: Calphad simulation, processing and characterization.* Acta Materialia, **to be published**.

[10] Couzinié, J.P., L. Lilensten, Y. Champion, G. Dirras, L. Perrière, and I. Guillot, *On the room temperature deformation mechanisms of a TiZrHfNbTa refractory high-entropy alloy.* Materials Science and Engineering: A, **2015**. 645: p. 255-263.

[11] Dirras, G., L. Lilensten, P. Djemia, M. Laurent-Brocq, D. Tingaud, J.P. Couzinié, L. Perrière, T. Chauveau, and I. Guillot, *Elastic and plastic properties of as-cast equimolar TiHfZrTaNb high-entropy alloy.* Materials Science and Engineering: A, **2016**. 654: p. 30-38.

[12] Gali, A. and E.P. George, *Tensile properties of high- and medium-entropy alloys.* Intermetallics, **2013**. 39 (0): p. 74-78.

[13] Gludovatz, B., A. Hohenwarter, D. Catoor, E.H. Chang, E.P. George, and R.O. Ritchie, *A fracture-resistant high-entropy alloy for cryogenic applications.* Science, **2014**. 345 (6201): p. 1153-1158.

[14] Otto, F., A. Dlouhý, C. Somsen, H. Bei, G. Eggeler, and E.P. George, *The influences of temperature and microstructure on the tensile properties of a CoCrFeMnNi high-entropy alloy.* Acta Materialia, **2013**. 61 (15): p. 5743-5755.

[15] Senkov, O.N., G.B. Wilks, J.M. Scott, and D.B. Miracle, *Mechanical properties of Nb25Mo25Ta25W25 and V20Nb20Mo20Ta20W20 refractory high entropy alloys.* Intermetallics, **2011**. 19 (5): p. 698-706.

[16] Zhang, Y., Y.J. Zhou, J.P. Lin, G.L. Chen, and P.K. Liaw, *Solid-solution phase formation rules for multi-component alloys.* Advanced Engineering Materials, **2008**. 10 (6): p. 534-538.

[17] Pickering, E.J. and N.G. Jones, *High-entropy alloys: a critical assessment of their founding principles and future prospects.* International Materials Reviews, **2016**. 61 (3): p. 183-202.

[18] Owen, L.R., E.J. Pickering, H.Y. Playford, H.J. Stone, M.G. Tucker, and N.G. Jones, *An assessment of the lattice strain in the CrMnFeCoNi high-entropy alloy.* Acta Materialia, **2017**. 122: p. 11-18.

[19] Deng, Y., C.C. Tasan, K.G. Pradeep, H. Springer, A. Kostka, and D. Raabe, *Design of a twinning-induced plasticity high entropy alloy.* Acta Materialia, **2015**. 94 (0): p. 124-133.

[20] Yao, M.J., K.G. Pradeep, C.C. Tasan, and D. Raabe, *A novel, single phase, non-equiatomic FeMnNiCoCr high-entropy alloy with exceptional phase stability and tensile ductility.* Scripta Materialia, **2014**. 72–73 (0): p. 5-8.

[21] He, J.Y., W.H. Liu, H. Wang, Y. Wu, X.J. Liu, T.G. Nieh, and Z.P. Lu, *Effects of Al addition on structural evolution and tensile properties of the FeCoNiCrMn high-entropy alloy system.* Acta Materialia, **2014**. 62 (0): p. 105-113.

[22] Pradeep, K.G., C.C. Tasan, M.J. Yao, Y. Deng, H. Springer, and D. Raabe, *Non-equiatomic high entropy alloys: Approach towards rapid alloy screening and property-oriented design.* Materials Science and Engineering: A, **2015**. 648: p. 183-192.

[23] Laurent-Brocq, M., L. Perrière, R. Pirès, and Y. Champion, *From high entropy alloys to diluted multi-component alloys: domain of existence of a solid-solution.* Materials & Design. accepted.

[24] Maier-Kiener, V., B. Schuh, E.P. George, H. Clemens, and A. Hohenwarter, *Nanoindentation testing as a powerful screening tool for assessing phase stability of nanocrystalline high-entropy alloys.* Materials & Design, **2017**. 115: p. 479-485.

[25] Laurent-Brocq, M., E. Béjanin, and Y. Champion, *Influence of roughness and tilt on nanoindentation measurements: A quantitative model.* Scanning, **2015**. 9999: p. 1-11.

[26] Nix, W.D. and H. Gao, *Indentation size effects in crystalline materials: A law for strain gradient plasticity.* Journal of the Mechanics and Physics of Solids, **1998**. 46 (3): p. 411-425.

[27] Oliver, W.C. and G.M. Pharr, *Measurement of hardness and elastic modulus by instrumented indentation: Advances in understanding and refinements to methodology.* Journal of Materials Research, **2004**. 19 (01): p. 3-20.

[28] Pearson, W.B., *A handbook of lattice spacings and structures of metals and alloys*. International series of monographs in metal physics and physical metallurgy, ed. G.V. Raynor. Vol. 2. **1967**, Oxford: Pergamon Press.

[29] Varvenne, C., A. Luque, and W.A. Curtin, *Theory of strengthening in fcc high entropy alloys.* Acta Materialia, **2016**. 118: p. 164-176.

[30] King, H.W., *Quantitative Size-Factors for Metallic Solid Solutions.* Journal of Materials Science, **1966**. 1 (1): p. 79-90.

[31] Toda-Caraballo, I. and P.E.J. Rivera-Díaz-del-Castillo, *Modelling solid solution hardening in high entropy alloys.* Acta Materialia, **2015**. 85 (0): p. 14-23.

[32] Jin, K., S. Mu, K. An, W.D. Porter, G.D. Samolyuk, G.M. Stocks, and H. Bei, *Thermophysical properties of Ni-containing single-phase concentrated solid solution alloys.* Materials & Design, **2017**. 117: p. 185-192.

[33] Lucas, M.S., G.B. Wilks, L. Mauger, J.A. Muñoz, O.N. Senkov, E. Michel, J. Horwath, S.L. Semiatin, M.B. Stone, D.L. Abernathy, and E. Karapetrova, *Absence of long-range chemical ordering in equimolar FeCoCrNi.* Applied Physics Letters, **2012**. 100 (25): p. -.

[34] Smith, T.M., M.S. Hooshmand, B.D. Esser, F. Otto, D.W. McComb, E.P. George, M. Ghazisaeidi, and M.J. Mills, *Atomic-scale characterization and modeling of 60° dislocations in a high-entropy alloy.* Acta Materialia, **2016**. 110: p. 352-363.

[35] Tamm, A., A. Aabloo, M. Klintenberg, M. Stocks, and A. Caro, *Atomic-scale properties of Ni-based FCC ternary, and quaternary alloys.* Acta Materialia, **2015**. 99: p. 307-312.

[36] Durst, K., O. Franke, A. Böhner, and M. Göken, *Indentation size effect in Ni–Fe solid solutions.* Acta Materialia, **2007**. 55 (20): p. 6825-6833.

[37] Gludovatz, B., A. Hohenwarter, K.V.S. Thurston, H. Bei, Z. Wu, E.P. George, and R.O. Ritchie, *Exceptional damage-tolerance of a medium-entropy alloy CrCoNi at cryogenic temperatures.* Nature Communication, **2016**. 7.

[38] Wu, Z., H. Bei, G.M. Pharr, and E.P. George, *Temperature dependence of the mechanical properties of equiatomic solid solution alloys with face-centered cubic crystal structures.* Acta Materialia, **2014**. 81 (0): p. 428-441.

[39] Nabarro, F.R.N., *The theory of solid solution hardening.* Philosophical Magazine **1977**. 35 (3): p. 613-622.

[40] Tabor, D., *Hardness of metals*. **1951**, Oxford: Clarendon Press.

[41] Fischer-Cripps, A.C., *Analysis of nanoindentation test data*, in *Nanoindentation*. **2011**, Springer: New York, USA. p. 39.

[42] Haglund, A., M. Koehler, D. Catoor, E.P. George, and V. Keppens, *Polycrystalline elastic moduli of a high-entropy alloy at cryogenic temperatures.* Intermetallics, **2015**. 58 (0): p. 62-64.

[43] Pearson, W.B., *A handbook of lattice spacings and structures of metals and alloys*. International series of monographs in metal physics and physical metallurgy, ed. G.V. Raynor. Vol. 1. **1958**, Oxford: Pergamon Press.